Nuclear Instruments and Methods in Physics Research A288 (1990) 477–485
North-Holland

A VERSATILE DOUBLE-AXIS MULTICOUNTER NEUTRON POWDER DIFFRACTOMETER

J. SCHEFER [1], P. FISCHER [2], H. HEER [2], A. ISACSON [2], M. KOCH [2] and R. THUT [2]

[1] *Condensed Matter Research and Materials Sciences, Paul Scherrer Institute, CH-5232 Villigen PSI, Switzerland*
[2] *Laboratory for Neutron Scattering, ETH, Zürich, CH-5232 Villigen PSI, Switzerland*

Received 26 September 1989

The double-axis multicounter diffractometer (DMC) installed at the 10-MW reactor SAPHIR (PSI) has been designed as a good-flux, good-resolution (presently $\Delta d/d \geq 4\times10^{-3}$) neutron powder diffractometer. The detector bank is based on a commercial position-sensitive linear BF_3 detector which may be automatically and precisely positioned on air cushions (standard epoxy floor). Vertically variable focusing germanium or pyrolythic graphite monochromators are used. Special efforts were made to optimize the sample environment, e.g. by developing an oscillating radial collimator system. Although the monochromator shielding is not yet in a final state, the diffractometer is successfully operating since several years. Design properties and operational experience are discussed. Online data analysis based on LSI and VAX computers is facilitated by user-friendly software.

1. Introduction

With an optimized spectrometer, neutron powder diffraction is a powerful tool to investigate structure and magnetic ordering phenomena in condensed matter. The applications range from solid state physics, chemistry, crystallography, materials science to biology and cover both fundamental and applied research. Such an instrument may also be used for amorphous, quasicrystalline and liquid specimens.

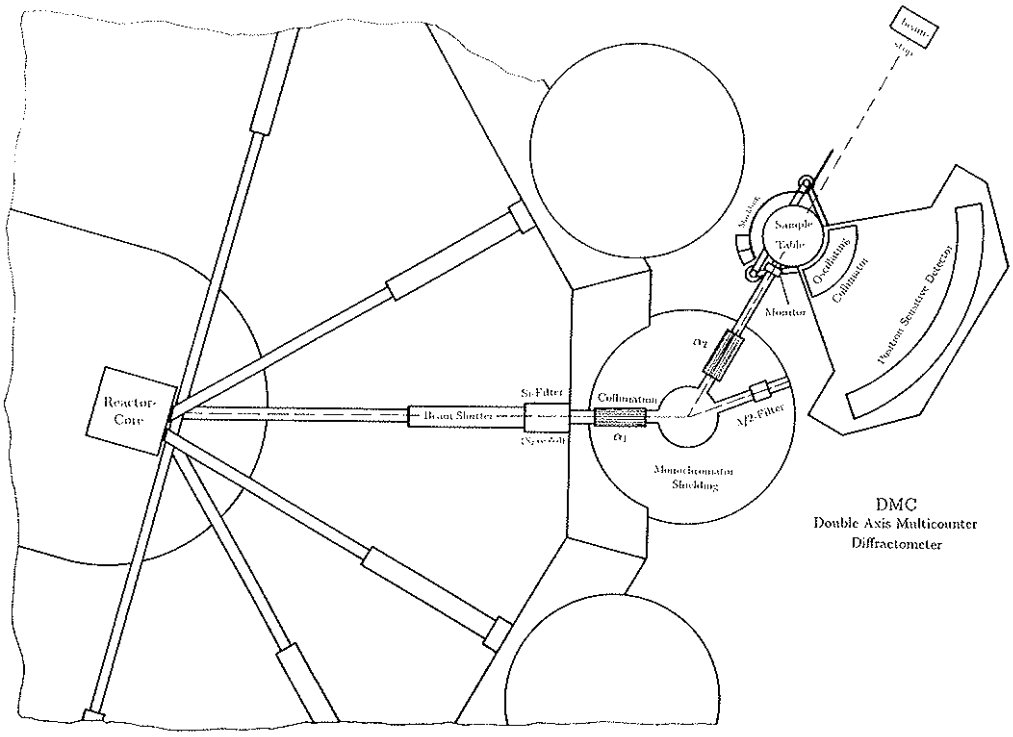

Fig. 1. Present state of the double-axis multicounter powder diffractometer DMC at the reactor SAPHIR.

0168-9002/90/$03.50

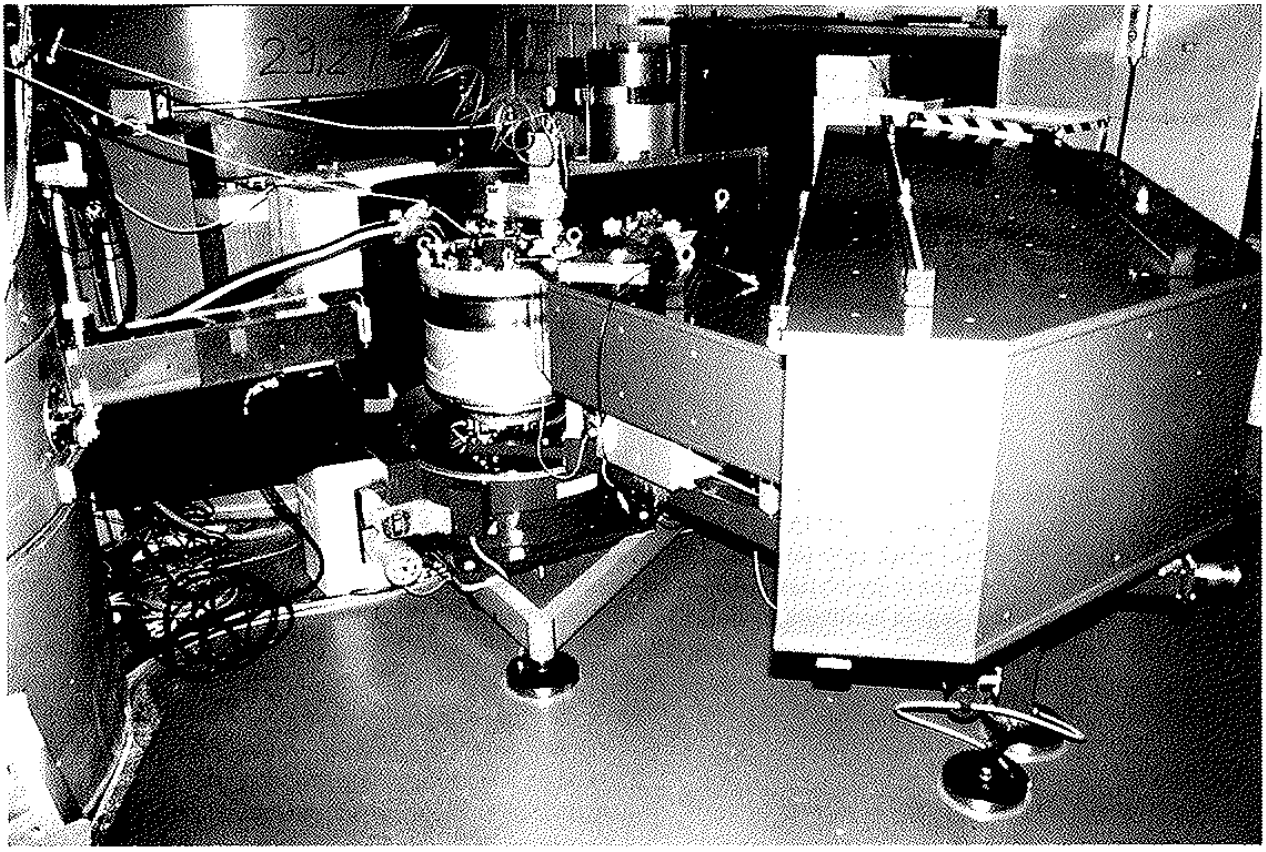

Fig. 2. Present state of the double-axis multicounter powder diffractometer DMC at the reactor SAPHIR.

An obvious way to use a continuous neutron source such as the 10-MW light-water reactor SAPHIR or the spallation source SINQ (in construction) efficiently is the application of focusing monochromators and multidetectors. Figs. 1 and 2 give an overview of our DMC diffractometer, which was put into operation in 1984 (see preliminary reports [1,2]).

This instrument is based on a linear position-sensitive BF_3 counter with 400 wires [3,4]. Presently it is installed at the radial thermal beam tube R4 at the reactor SAPHIR (PSI Villigen), equipped with a liquid-nitrogen-cooled silicon filter [5]. Design considerations of general interest and practical experience are summarized within this report.

2. Diffractometer design

Subsequently a description of the major components used in the diffractometer is given.

2.1. Beam shutter / filter / monochromator-shielding

The monochromator is mounted in a steel/concrete shielding of 100 cm radius at a distance of 530 cm from the reactor core on the radial thermal beam tube R4 of the reactor SAPHIR. The beam tube may be opened/closed by a special shutter system [5].

A liquid-nitrogen-cooled Si-filter [5,6] is reducing essentially the γ and fast-neutron flux, while absorbing about 25% of the thermal neutrons at 1.7 Å. For this purpose, a cylindrical perfect Si-single crystal (25 cm long, 9 cm diameter), sealed in a 0.1 cm steel container, is cooled by a liquid nitrogen bath. Levels are controlled by thermoelements and are automatically kept within certain limits.

2.1.1. Collimation

Three collimations may be used in powder diffraction: The primary collimation α_1 between the reactor core and the monochromator, α_2 between the monochromator and the sample and α_3 in front of the detector.

The white beam is collimated to $\alpha_1 = 10'$ (standard) or $\approx 40'$ in the high flux mode. The beam size is presently reduced to 5 cm height and 2 cm width. A new monochromator shielding is in planning. Its major features will be higher and variable take-off angles (up to about 90°), the use of the full 8 cm beam height and a variable primary collimation system (α_1). The latter system will allow fast adjustment of the resolution function to the problem studied (e.g. increasing the primary collimation α_1 from $10'$ to $40'$ yields an intensity gain of about a factor of three without considerable loss in resolution at low scattering angles; this is a favourable setup for the investigation of magnetic su-

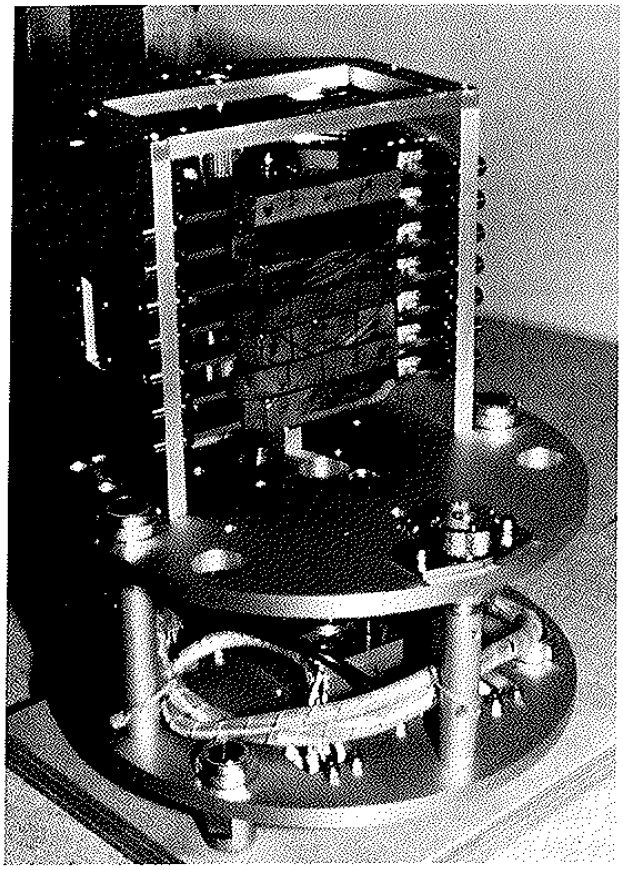

Fig. 3. Vertically focusing Ge monochromator, permitting individual orientation of each crystal slab.

perstructures). The higher monochromator take-off angles shift the resolution maximum to higher 2θ values and increase resolution for fixed collimation.

2.1.2. Monochromator crystals

The collimated white beam is monochromatized by a variable focusing germanium monochromator (311, 511 and other *hkk* reflections may be set up by a rotation in ω_{monochr}) or may be replaced by a pyrolythic graphite monochromator (002 reflection in connection with a 5 to 7 cm thick pyrolythic graphite filter). The main advantages of germanium are the essential reduction of higher-order contamination ($\lambda/2$) and better resolution compared with graphite. Disadvantages are the technical difficulties in obtaining a large homogeneous Gaussian mosaic distribution and the smaller reflectivity. In future also a double system for simple computer-controlled replacement of these two monochromators is envisaged.

The vertically focusing Ge monochromator has been developped and installed recently (cf. fig. 3). The monochromator used in reflecting position consists of 7 Ge single crystals of 1.2 cm height, 1.0 cm thickness and 6.5 to 7.5 cm width with (311) planes parallel to the reflecting surface. Each crystal slab may be individually directed in three directions by adjusting screws. The slabs were cut according to a vertical [0$\bar{1}$1] axis to enable use of different *hkk* planes. The horizontal mosaic spread is about 17′ and the vertical one 4′ [7]. A motor/digitizer system is capable of adjusting them simultaneously to a pseudo-parabolic shape. More detailed information has been published in ref. [8]. A similar system for pyrolythic graphite has been described in [9]. The monochromator is adjusted by a 3-point support to the monochromator table. The flux gain due to this system is approximately 2.5 with no change in the resolution function. The use of the full beam height is expected to increase this value further. The Ge monochromator shows good peak shapes even at scattering angles of 130° at a wavelength $\lambda = 1.7$ Å.

Normally no secondary collimation α_2 is installed, as this results mainly in an intensity loss. However, the best resolution is obtained with $\alpha_1 \approx 2\alpha_2$. The ternary collimation is given by the geometry of the fixed detector radius (150.0 cm) and the distance between the vertical tungsten wires (0.53 cm) as $\alpha_3 = 12'$. The sample diameter for best resolution is therefore 0.53 cm. However, a sample diameter of 0.8 cm has been proven to be a good compromise between counting statistics and resolution (factor 2.5 gain of intensity due to increase of volume). The effective collimation α_3 is given by

$$\alpha_3 = \tan^{-1}\left(\frac{0.53 + \varnothing_s[\text{cm}]}{2 \times 150.0}\right), \tag{1}$$

e.g. $\alpha_3 = 12$, 15, 18 and 23′ for sample diameters $\varnothing_s =$ 0.5, 0.8, 1.0 and 1.5 cm respectively.

2.2. Sample environment

As the detector has a full 80° opening to the sample, containment walls around the sample yield disturbing Bragg peaks in the diffraction pattern. Therefore great care has been taken to build a steel container of 48 cm diameter and 36 cm height to support all the auxiliary equipment such as a closed-cycle He refrigerator etc., while being evacuated to avoid air scattering. This vessel is equipped with a 6 cm high bent vanadium window with 355° access. A magnetic liquid seal on the top allows oscillation of the cooling machines or ovens by maximal ±90° (cf. figs. 2 and 4), thus reducing preferred orientation effects. The inside is covered with cadmium. Additional slits reduce diffuse scattering in front of the sample. An additional shielding of 0.5-cm 50%-borated araldite plates as well as a 20 cm wall of borated paraffine blocks at the right side to the sample is necessary for shielding the detector to the reactor and the neighbour spectrometer.

At present, the temperature available on the DMC spectrometer ranges from approximately 7 mK to 1500 K.

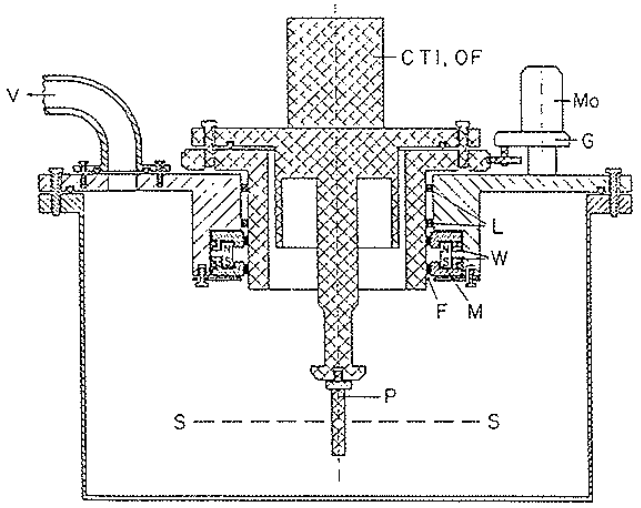

Fig. 4. Vertical cut through the rotation-mounting of a closed-cycle He refrigerator, in the evacuated sample vessel. Major parts are: CTI = He refrigerator, Mo = motor, F = magnetic liquid, M = permanent magnet, P = sample can, S-S = scattering plane, V = vacuum-pump line.

2.3. Oscillating collimator system

An oscillating collimator has been recently installed between sample and detector to avoid Bragg scattering from cryostats and furnaces, such as our Al/Ta high-temperature radiation oven (maximum 1500 K). Compared to the also available V furnance the peak-to-background ratio is thus essentially improved.

The collimator (cf. fig. 5) has an inner radius of 25.5 cm and an outer radius of 45.0 cm. The angular distance between the 73 cadmium coated steel plates (19.4 cm long and 6.4 cm high) of 0.02 cm thickness is 1.2° (both sides are coated with 0.008 cm of cadmium). The principle of the system is similar to the one described in ref. [10]. The collimator is moved on three steel spheres in 2000 microsteps according to variable speed (≤ 240 steps s^{-1}) within $2 \times 1.2°$. The end positions are defined by accurate microswitches (adjustable positions). To obtain a uniform distribution of the blade positions, the end positions are measured twice and set exactly to the position of a blade. The collimator moves independently of the measurement, except for occasional adjustment of the speed. Fig. 6 shows the difference between a measurement of a UCu_5 sample in a dilution cryostat with and without this collimator system. It absorbs about 21% of the neutrons, but yields also a corresponding background reduction by a factor of 2.75. The oscillating background in fig. 6c is caused by the cadmium-coated blades of the nonoscillating collimator.

2.4. Detector system

The detector bank is moved on air cushions, allowing a free rotation around the sample table. Depending on the distance monochromator–sample, scattering angles 2Θ up to 160° may be reached ($2\Theta_{max} = 135°$ for a distance of 215 cm).

The shielding consists of a self-supporting sandwich construction of plastic (2.5 cm), polyethylene (2.5 cm), 5%-borated polyethylene (2.5 cm), 50%-borated araldite (0.5 cm) and cadmium (0.1 cm). It is mounted on a steel support, and connected by two turn points to the sample table, thus avoiding mechanical stress. Motor and absolute decoder of the 2θ arm are running on two

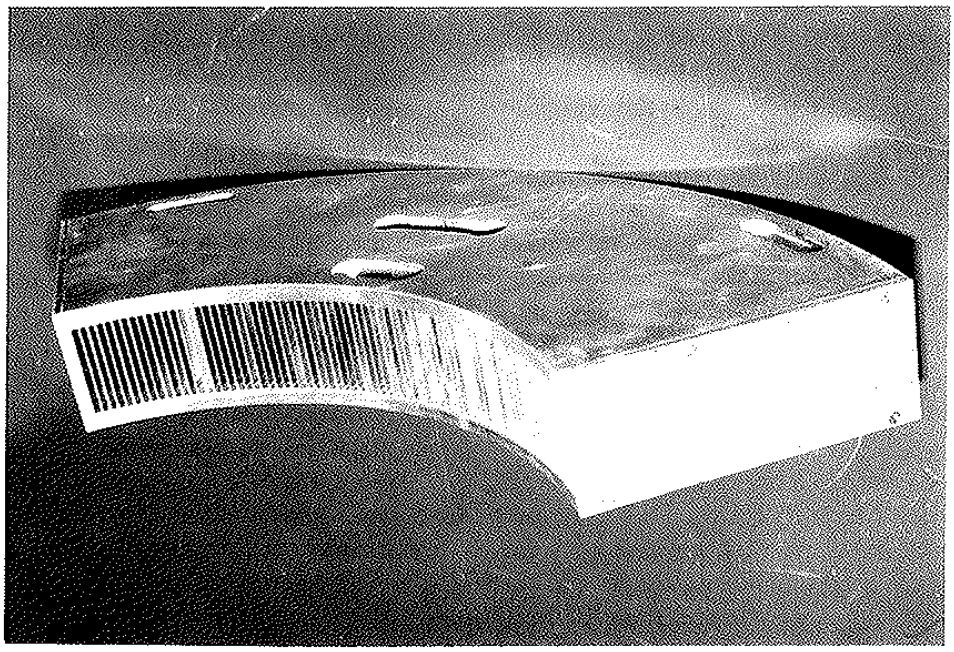

Fig. 5. Oscillating collimator system.

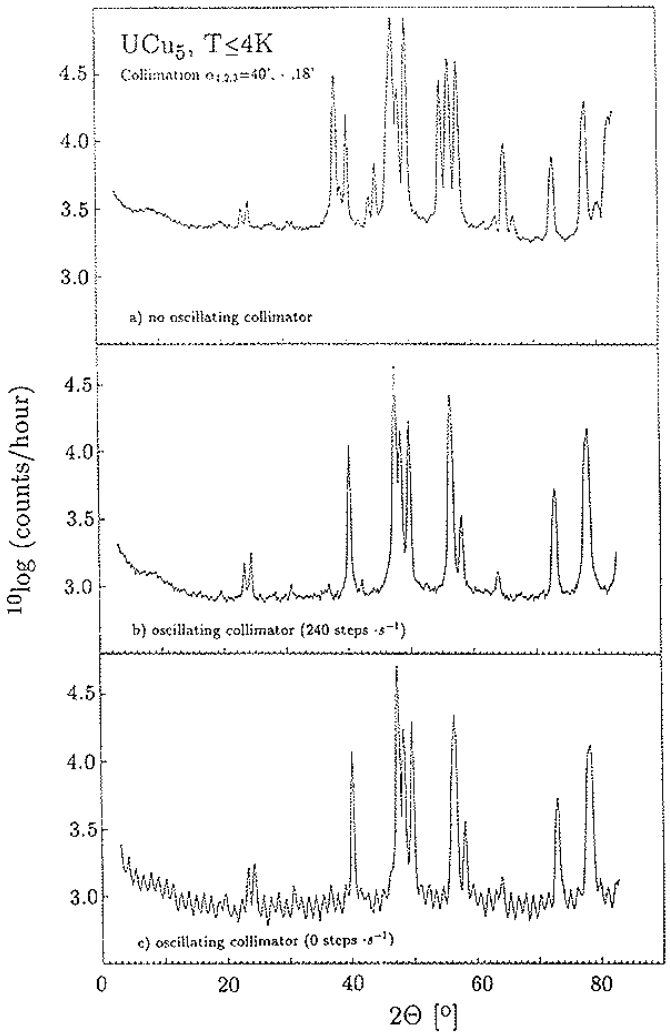

Fig. 6. Diffraction pattern of UCu_5 at 4 K in a dilution cryostat without (a) and with (frequency = 240 steps s^{-1} (b) and 0 steps s^{-1} (c)) oscillating collimator. Maximum peak intensity is 8.4×10^4 (measurement time: 1 h, $\lambda = 1.703$ Å, collimation $\alpha_{1,2,3} = 40'-18'$) (P. Böni, unpublished).

separate bearings, allowing reproducible positioning with an accuracy better than 0.01°.

The detector system is based on a commercially available BF_3 linear position-sensitive counter (LCC 400CP, Thompson-CSF), covering simultaneously a scattering angle range of 79.8°, corresponding to 400 detectors with angular separation of 0.2° and a radius of 150 cm. For this detector a special arrangement of anodes/cathodes is used in order to reduce the electronic counting chains (preamplifiers etc.) from 400 down to 40 (20 × 20). The design has been described in refs. [3,4]. The detector logic outputs a 9-bit digital signal for every neutron detected, decoding the position. This signal is transferred by an in-house built device to a histogram memory (Camac, LeCroy) and simultanously to a multichannel display (MCA ND62). The detector is mounted electronically isolated from the diffractometer.

2.5. Control / Data handling

The system is controlled by an LSI 11/23 computer with a 10-MB winchester and one floppy disk. Camac interfaces are used to access the peripheral interfaces. Absolute decoders are used for angle readout. Also sample temperature may be set and checked by the spectrometer program.

Generally, measurements at four scattering angle starting positions such as $2\Theta = 3.0$, 3.1, 55.0 and 55.1° are repeated several times until the desired counting statistics is reached. The standard step in 2θ is 0.1°. The angular step of $\Delta 2\Theta \leq 0.1°$ is necessary in order to obtain a sufficient number of profile points in the Bragg peaks. Even step 0.05° showed no deviation of Bragg reflections from Gaussian form due to malpositioning (cf. insert in fig. 9).

Table 1
Presently available DMC diffractometer setups; + means not used/measured

Primary filter	N_2-cooled Si, 25 cm					
Primary collimation [′] α_1	10–40					
Ternary collimation [′] α_3	≥12					
Sample diameter [cm]	0.5–1.5					
Beam height [cm]	≤5.0					
Temperature range [K]	0.007–1500					
Monochromator	Ge				C	
Focusing	bent/variable				bent/fixed	
Bragg reflection	(311)		(511)		(002)	
$2\Theta_{mono}$ [°]	40.8	60.0	40.8	60.0	40.8	60.0
Wavelength λ [Å]	1.17	1.71	0.74	1.09	2.3	3.36
C-filter [cm]	none	none	none	none	6.55	+
λ/2 [%]	+	0.8	+	+	1	+
Flux after Si-filter sample [10^8 n cm^{-2} s^{-1}]	+	4.1	+	+	+	+
Flux at sample [10^6 n cm^{-2} s^{-1}] ($\alpha_1 = 10'$)	+	0.5	+	+	+	+

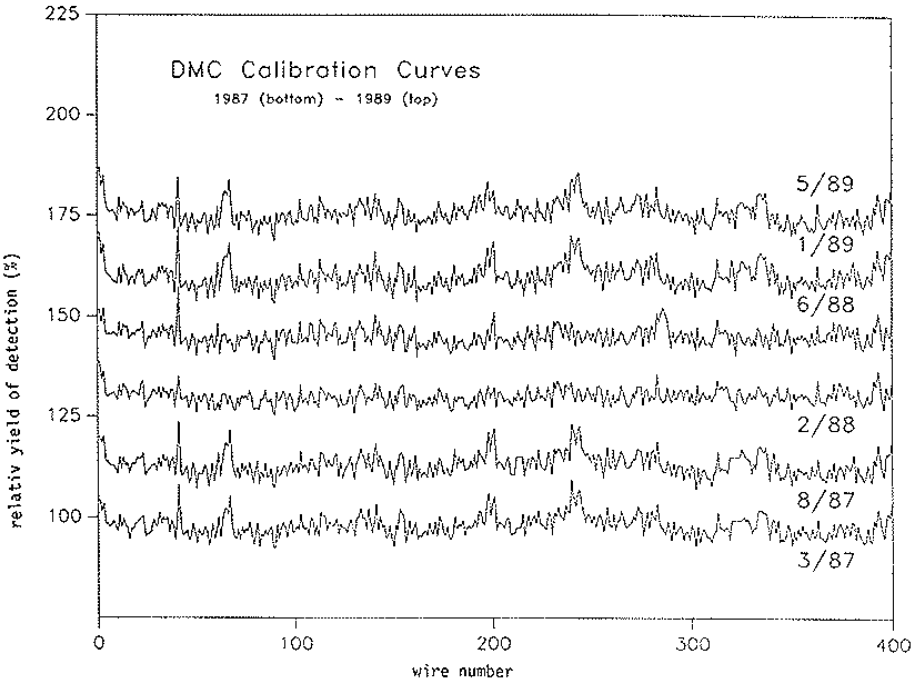

Fig. 7. Calibration curves in 1987 (bottom line) and 1989 (top line). Lines are shifted for better comparison by 15% from curve to curve.

The profile intensities of the different scans are saved on the winchester disk. Each run may be inspected anytime on a graphic terminal with access to the computer network. They are summed, calibrated and corrected for monitor, absorption on the LSI in one step. Various interactive self-explaining Fortran programs are available. The final diffraction pattern is analysed by various Rietveld [11,12] packages on VAX computers. A list of different programs is available on request. Data are transfered by DECNET, local area networks or BITNET. Direct control of running measurements (diffraction pattern, temperature, etc.) or data

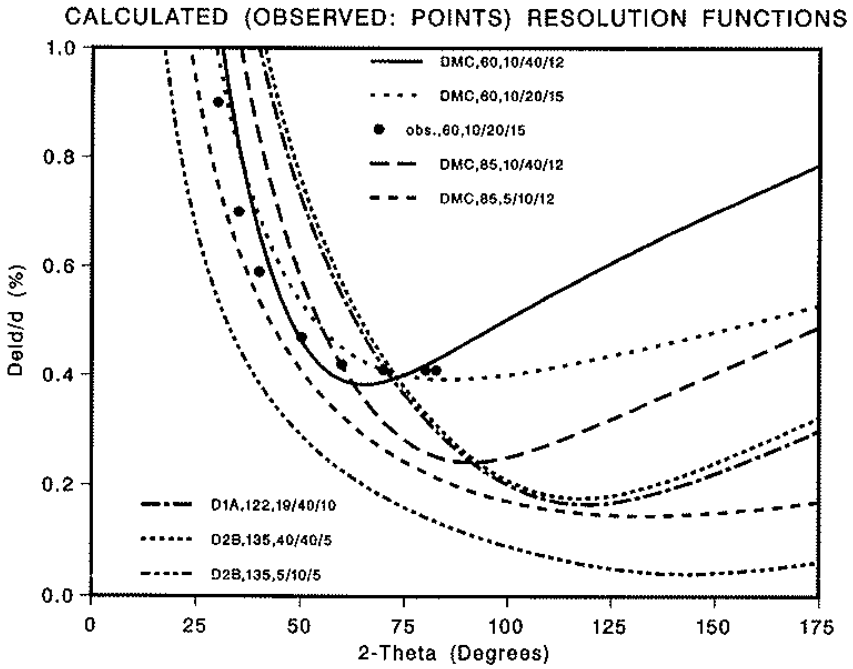

Fig. 8. Calculated resolutions of DMC compared to those of D1A and D2B. Legends: Spectrometer, $2\Theta_{monochr}$ [deg] and collimations α_1, α_2, α_3 [′].

Table 2
Calculated and observed best resolutions and intensities ("luminosity" not corrected for wavelength dependence of monochromator, sample reflectivities, and detector yield) for various neutron powder diffractometer configurations. Different values such as best resolution $\Delta d/d$ (d = interplanar spacing), corresponding peak halfwidth (HW), 2Θ position for different parameters of collimation $\alpha_{1,2,3}$, monochromator angle $2\Theta_{mono}$, monochromator mosaic β_M and different monochromator planes are listed.

$2\Theta_{mono}$ [°]	Mono-chromator	λ [Å]	α_1 [′]	α_2 [′]	α_3 [′]	β_M [′]	HW for d_{opt} [°]	d_{opt} [Å]	$\Delta d/d$ optimal [10^{-3}]	2Θ minimal [°]	Relative intensity [arb.]	d_{min} for $2\Theta = 160°$ [Å]
18.0	C_{002}	1.05	10	50	20	40	0.44	2.69	19.2	23	34	0.53
18.0	C_{002}	1.05	50	10	20	40	2.94	0.98	40.3	65	34	0.53
40.8	C_{002}	2.34	20	50	30	40	0.58	2.53	12.7	55	100	1.19
40.8	C_{002}	2.34	40	40	12	40	0.59	3.59	15.0	38	100	1.19
40.8	C_{002}	2.34	20	40	12	40	0.40	3.23	8.9	43	34	1.19
40.8	Ge_{311}	1.19	10	40	12	20	0.28	1.55	6.0	45	13	0.60
60.0	Ge_{311}	1.71	40	40	12	20	0.42	2.12	8.3	48	44	0.87
60.0	Ge_{311}	1.71	10	40	23	20	0.54	1.29	5.4	83	26	0.87
60.0	Ge_{311}	1.71	10	40	18	20	0.40	1.44	4.8	73	20	0.87
60.0	Ge_{311}	1.71	10	40	15	20	0.33	1.53	4.3	68	17	0.87
60.0	Ge_{311}	1.71	10	40	12	20	0.28	1.59	3.8	65	13	0.87
60.0	Ge_{311}	1.71	10	20	15	20	0.41	1.26	3.9	85	10	0.87
60.0	Ge_{311}	1.71	10	40	12	10	0.29	1.54	3.8	68	8	0.87
60.0	Ge_{511}	1.09	30	40	12	20	0.28	1.01	3.8	65	13	0.55
85.0	Ge_{511}	1.47	10	40	12	20	0.28	1.03	2.4	91	13	0.75
85.0	Ge_{511}	1.47	5	10	12	20	0.38	0.80	1.5	133	2	0.75
90.0	Ge_{311}	2.41	20	40	12	20	0.37	1.74	3.3	88	26	1.22
90.0	Ge_{311}	2.41	10	40	12	20	0.28	1.64	2.2	95	13	1.22
122.0	Ge_{511}	1.91	19	40	10	20	0.33	1.10	1.7	120	21	0.97
135.0	Ge_{533}	1.59	40	40	5	20	0.33	0.93	1.8	118	19	0.81
135.0	Ge_{533}	1.59	5	40	5	20	0.12	0.86	0.4	136	3	0.81
135.0	Ge_{533}	1.59	5	10	5	20	0.14	0.84	0.4	144	1	0.81
135.0	Ge_{755}	1.05	5	10	5	20	0.14	0.55	0.4	144	1	0.59
165.0	Ge_{533}	1.71	5	10	5	20	0.14	0.86	0.1	168	1	0.87

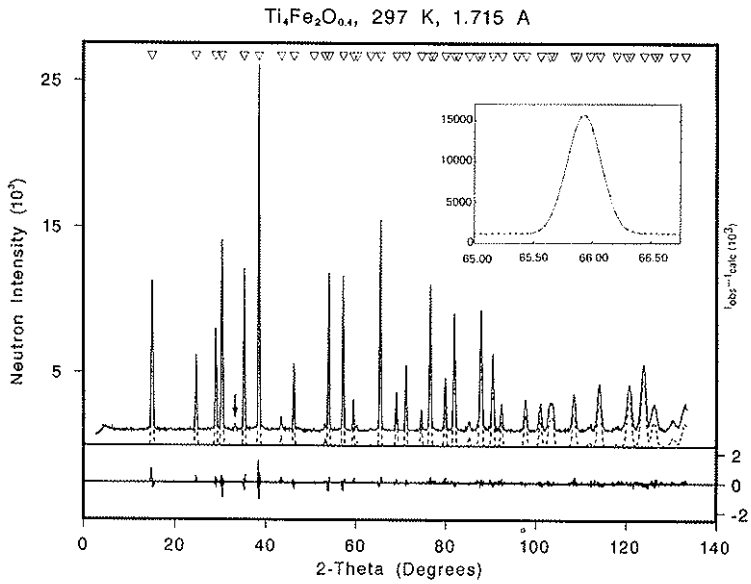

Fig. 9. Observed (full) and calculated (dashed line) neutron diffraction pattern of cubic ($a_0 = 11.333$ Å) $Ti_4Fe_2O_{0.4}$, measured on DMC. The arrow indicates the only weak additional TiFe (100) peak. $\varnothing_{sample} = 1.0$ cm, $\Delta_{2\Theta} = 0.05°$. $\lambda = 1.715$ Å, $2\Theta_{mono} = 60.0°$, $\alpha_1 = 10'$, $\alpha_2 = 40'$, $\alpha_3 = 18'$ [16]. The insert illustrates the Gaussian Bragg peak shape.

processing is possible via KOMETH (broad band network) or phone.

3. Instrumental performance

3.1. Detector calibration

Diffraction patterns have to be corrected for the varying yield of detection of the different wires and differences in the electronics. For this purpose, a vanadium single crystal of 0.7 cm diameter and 4.5 cm height is exposed to the neutron beam (30 h at 20 K, background measurements are usually not necessary) with primary collimation $\alpha_1 \approx 40'$ (high intensity mode). Use of V powders or direct beam methods should be avoided. Powder methods have been used until 1987. Therefore, this calibration curves show problems in the region of the vanadium Bragg reflections (cf. fig. 7). Differences are also due to replaced electronic components. The electronic background per channel is better than 0.01 counts/min, the background at 10 MW reactor power 0.1 counts/min per wire.

The detector is very stable, as illustrated in fig. 7. Thus, calibration is repeated generally only two or three times a year.

3.2. Resolution / flux

The tables give an overview on the presently possible (table 1) and future monochromator configurations (table 2). Flux measurements have been done with a primary collimation $\alpha_1 = 10'$.

At present the diffractometer resolution $\Delta d/d$ (d is interplanar lattice spacing) attains 4×10^{-3}, compared to 2×10^{-3} of D1A and $(0.5\text{–}2) \times 10^{-3}$ of D2B *. With larger monochromator take-off angles the latter values could be approached, but at the reactor SAPHIR space and neutron flux limitations restrict the possibilities.

3.3. Profile refinement example

Profile refinement has been performed successfully on many samples. As an illustration we show in fig. 9 the result performed recently on $Ti_4Fe_2O_{0.4}$ [16].

4. Discussion

The DMC powder diffractometer shows, that good resolution (cf. fig. 8) and good intensity can be reached even on a medium-flux reactor by optimizing collimation, using focusing monochromators, linear position-sensitive detectors of reasonable size and taking care of the design of each additional component. Advanced data processing allows even to an unexperienced user to run the instrument without major difficulties. This is especially essential as the mean measurement time for a diffraction pattern of good counting statistics in case of a 2.5 cm^3 sample is only about 1 day. Quick sample tests are already possible within several minutes. With a pyrolythic graphite monochromator set to a wavelength $\lambda = 2.4$ Å, real-time experiments (≥ 5 min) are feasible similar to D1B/ILL. Compared to high-resolution multi-Soller systems such as D2B/ILL [17] a disadvantage of a linear position-sensitive detector as DMC is the coupling of resolution and sample diameter. This might perhaps be overcome by a special oscillating collimator.

Future developments such as the ^{7}Li–glass scintillator systems [18] yielding greater sensitivity, higher resolution and increased number of simultanously measured profile points are promising possibilities for further optimization of similar neutron powder diffractometers.

* Fig. 8 compares the instrumental resolution of DMC to the high-resolution diffractometers D1A and D2B at ILL. Calculations were performed with program Presol [13], which is based on the resolution theory of Caglioti et al. [14,15].

Acknowledgements

We gratefully thank the ETH Zürich, the universities of Bern and Geneva, PSI and the Swiss National Science Foundation for financial support. We are indebted to Prof. W. Hälg, Prof. A. Furrer, Dr. W. Bührer, B. Bron et al. for their initial support and developments, local workshops and electronic laboratories at PSI, and the reactor department SAPHIR for important infrastructure contributions and flux measurements, and N. Frei for the sketch of the spectrometer.

We also appreciate the support from various institutions such as HMI Berlin (Dr. A. Axmann et al.), ILL Grenoble (Dr. A.W. Hewat), KFA Jülich (Prof. G. Will et al.) for the discussions on their experience with similar systems. In particular the generous assistance of the monochromator group of ILL (Dr. A. Freund et al.) should be mentioned.

References

[1] W. Hälg, H. Heer, J. Schefer, P. Fischer, B. Bron, A. Isacson and M. Koch, Helv. Phys. Acta 57 (1984) 741.
[2] P. Fischer, Neutron Diffraction Newsletter IUC (1985) 15.
[3] P. Lecuyer, Revue Technique Thomsen, CSF 9, no. 4 (1977).
[4] A. Axmann, in: Position Sensitive Detection of Thermal Neutrons, eds. P. Convert and J.B. Forsyth (Academic Press, 1983) 91.

[5] W. Bührer, V. Herrenberger, B. Hollenstein, M. Koch and A. Rüede, Nucl. Instr. and Meth. A236 (1985) 315.
[6] M. Brugger, Nucl. Instr. and Meth. 135 (1976) 289.
[7] A. Freund, Nucl. Instr. and Meth. 124 (1975) 93.
[8] P. Fischer, R. Thut, M. Koch, A. Isacson, W. Bührer, and P. Allenspach, Laboratory for Neutron Scattering, Progress Report 1988, LNS-146 (1989) 125.
[9] W. Bührer, R. Bührer, A. Isacson, M. Koch and R. Thut, Nucl. Instr. and Meth. 179 (1981) 259.
[10] A.F. Wright, M. Berneron and S.P. Heatman, Nucl. Instr. and Meth. 180 (1981) 655.
[11] H.M. Rietveld, J. Appl. Crystallogr. 2 (1969) 65.
[12] A.W. Hewat, Harwell report AERE-R7350 (1973).
[13] P. Fischer, Laboratory for Neutron Scattering, Progress Report 1987 LNS-137 (1988) 124.
[14] G. Caglioti, A. Paoletti, F.P. Ricci, Nucl. Instr. and Meth. 3 (1958) 223.
[15] A.W. Hewat, Nucl. Instr. and Meth. 127 (1975) 361.
[16] B. Rupp and P. Fischer, J. Less-Common Metals A144 (1988) 315.
[17] A.W. Hewat, in: High Resolution Powder Diffraction, ed. C.R.A. Catlow, Materials Science Forum 9 (1986) 69.
[18] W. Schäfer, E. Jansen, F. Elf and G. Will, J. Appl. Crystallogr. 17 (1984) 159.